CrystEngComm

Cite this: *CrystEngComm*, 2012, **14**, 2871

www.rsc.org/crystengcomm

PAPER

Facile growth of silver crystals with greatly varied morphologies by PEO-PPO-PEO tri-block copolymers

Jing-Cyuan Yang,[a] Chun-Hua Chen*[a] and Ren-Jye Wu[b]

Received 18th October 2011, Accepted 5th January 2012
DOI: 10.1039/c2ce06385a

Silver crystals with various novel nano-scale morphologies were synthesized from the reduction of silver nitrate ($AgNO_3$) by ascorbic acid (AsA) in aqueous PEO-PPO-PEO tri-block copolymer (F127) solutions. The presence of only high-concentration AsA at the very initial stage of reduction acts as a key factor in forming distinct branched quasi-spherical Ag nanocrystals where coral-like and houseleek-like morphologies can be kinetically controlled *via* subsequent addition of F127. When AsA and F127 were mixed before the reduction, three-dimensional dendritic Ag nanocrystals with highly ordered dendrites were largely obtained. In contrast to these branched crystals prepared under low F127 concentration, the face-centered cubic (FCC) packed micelles at high F127 concentration, which provided orderly reaction spaces for $AgNO_3$ and AsA reagents, dominated the growth of triangular and hexagonal prisms. The great variety in morphology is directly correlated with not only the concentration ratio between these reactants but the F127 induced kinetic mechanisms. Moreover, the greatly branched Ag nanocrystals exhibit significant surface-enhanced Raman scattering (SERS) for facilely, rapidly and effectively determining malachite green oxalate (MG) in aqueous solution. The present results provide valuable data not only for fundamental understanding of the directing effect of both F127 and AsA on the synthesis of Ag nanocrystals, but for advanced design and practical manufacturing of metals enhanced SERS sensors.

Introduction

Silver micro/nano-structures with various sizes, dimensions and morphologies have been widely designed, produced, investigated and subsequently applied to a variety of fields in the past few decades. Among these research categories, synthesis of novel structures is always the most important and interesting topic because it is the threshold to explore distinct physical and chemical phenomena and fundamentals of nanoscience. Silver is especially attractive from both academic and industrial viewpoints since it not only exhibits many distinguishing characteristics for practical applications (*e.g.*, excellent thermal and electrical conductivity with any kind of scale and morphology for conducting adhesives, and the surface plasmonic resonance located in the visible region of colorimetric sensors), but can also be the best galvanic template for many advanced metallic structures due to its appropriate chemical reduction potential and easily controllable structures.

The most common and simplest way to synthesize well-dispersed Ag nanostructures or their assemblies can be achieved *via* direct chemical reduction of silver precursors, *e.g.*, silver nitrate ($AgNO_3$) by sodium borohydride ($NaBH_4$) in aqueous solution with or without the presence of ionic or organic stabilizers or surfactants such as sodium dodecyl sulfate (SDS), poly(vinylpyrrolidone) (PVP) and cetyltrimethylammonium bromide (CTAB).[1–3] However, regardless of whether surfactants exist or not, this approach tends to form simpler Ag nanostructures with smoother surfaces in order to minimize the total surface energy (equilibrium condition). Thus, by this wet process, simpler zero-dimensional (0-D) particles, such as perfect spheres, decahedrons, and icosahedrons, 1-D rods, 2-D triangle prisms and 3-D cubes all with smoother surfaces, are frequently observed. For many applications, including sensors and catalysts, the highly branched Ag nanostructures with high surface-to-volume ratios are greatly beneficial due to the many porous stacks constructed by these self-grown 3-D branches. In addition, the sharp edges and corners derived from the branched structures are considered to exhibit higher activities for improving the catalytic performance. It has been reported that the use of ascorbic acid (AsA) as a weak reductant provides a way to form significantly branched Ag particles from the reduction of $AgNO_3$ aqueous solution.[4] Wang *et al.* experimentally demonstrated that the formation of branched structures is initiated from the Ag bulbous seeds, *i.e.*, the aggregation of a few fast-formed Ag nanoparticles

[a]*Department of Materials Science and Engineering, National Chiao Tung University, 1001 Ta-Hsueh Rd, Hsin-Chu, 30010, Taiwan, ROC. E-mail: ChunHuaChen@mail.nctu.edu.tw; Fax: +886-3-5724727; Tel: +886-3-5131287*
[b]*Material and Chemical Research Laboratories, Industrial Technology Research Institute, Hsin-Chu, 31040, Taiwan, ROC. E-mail: RJWu@itri.org.tw; Tel: +886-3-5912967*

with continuous selective growth at certain positions (the tips) of the seeds, and is very sensitive to reduction conditions, such as the AsA concentration or the molar ratio of AsA to $AgNO_3$.[5] It should be noted that excluding NaOH from controlling pH, as demonstrated by Fukuyo *et al.*,[6] and CTAB/SDS as surfactants with very specific AsA concentrations, as reported by Zheng *et al.*,[7] addition of polymer surfactants such as PVP are generally not permitted; otherwise, only the multifaceted particles will be formed.[5] All these results indicate that AsA is an effective reducing agent for the formation of unusually branched Ag structures with shorter (generally <500 nm) and irregular branches, and less highly ordered ones (second, third, or higher). Another effective synthetic strategy to generate highly branched structures requires the appearance of amphiphilic block copolymers (ABCs). ABCs generally act as both reductants and protective agents for producing dispersed metallic nanoparticles in the absence of extra reductants[8–11] and as morphology-tunable soft templates for mesoporous materials.[12–15]

PEO-PPO-PEO, one of the commercial tri-block copolymers, has been confirmed to form stable lamellar, hexagonal and cubic phases at specific concentration ranges.[16] The hydrophilic PEO block can slowly reduce Ag ions to Ag through oxidation of their oxyethylene groups.[17,18] However, the results of Gao *et al.* were surprising since they showed the tri-block copolymer of poly-(oxyethylene)-poly(oxypropylene)-poly(oxyethylene) (PEO-PPO-PEO) to act as a growth directing agent in the formation of branched Ag nanocrystals with long branches in contrast to the shorter ones induced by AsA.[19] Wang *et al.* also demonstrated the PEO-PPO-PEO-mediated synthesis of distinct Pt nanocrystals with short branches in the presence of AsA.[20] In our experience, Pt ions cannot be reduced by PEO-PPO-PEO without any additional reductant. Thus, even though the copolymer was used in their work, the reductant AsA probably dominated the growth of Pt nanocrystals and consequently the formation of shorter branches.

We may briefly conclude from the above results that the existence of only PEO-PPO-PEO tri-block polymers generally elicits a long-range anisotropic crystal growth, whereas the use of only AsA promotes a short-range one. In this study, to achieve the purpose of obtaining Ag crystals with greatly varied morphologies, we coupled the unique feature of PEO-PPO-PEO tri-block polymers (F127) and the reductant AsA, where F127 acted as the growth directors and surfactants and AsA the reductant. By adjusting the relative concentration of F127, AsA and Ag precursors and the reducing processes, the functions of both F127 and AsA were dynamically varied to produce various silver crystals from 3-D dendrites or polyhedrons to 2-D prisms. In addition, for demonstrating potentially distinct morphology-dependent properties, the surface-enhanced Raman scattering (SERS) effects of the as-prepared Ag branched nanocrystals on determining malachite green oxalate (MG), a widely used fungicide and antiseptic in aquaculture industries, were also investigated.

Experimental

Materials

The tri-block copolymer, Pluronic F127 ($EO_{100}PO_{70}EO_{100}$, M_w = 12 600 g mol^{-1}), $AgNO_3$, AsA ($C_6H_8O_6$), and MG ($[(C_{23}H_{25}N_2)\cdot(C_2HO_4)]_2\cdot C_2H_2O_4$) were purchased from Aldrich. All the starting chemicals were used as received without further purification.

Synthesis

First, a completely dissolved F127 aqueous solution (0.3 g F127 in 9 mL deionized water) was prepared by stirring for 24 h. A 0.035 g amount of AsA was then added to the prepared F127 solution with stirring for a further 20 min. To synthesize Ag nanostructures, 1 mL of 0.02 M $AgNO_3$ aqueous solution was dropped into the prepared mixed reductant solution under vigorous stirring for only 1 min, which gave the final molar ratio of 1 : 10 : 1 for F127 : AsA : $AgNO_3$. After that, the well mixed solution was immediately allowed to stand to maintain the reducing reaction for 24 h. The solution colour gradually changed from transparent to yellowish, indicating the successful reduction of Ag nanocrystals. All the above procedures were carried out at room temperature. In order to collect the yellowish precipitate, the reacted solution was centrifuged at 15 000 rpm for 30 min. In this work, the F127 and $AgNO_3$ concentration ratio was varied to investigate its effect on the morphology of the Ag nanocrystals grown. The specimens for SERS examinations were prepared by dispersing the water-suspended Ag nanocrystals into an aqueous solution of MG for 24 h where the final concentration of MG is 0.01 M. A droplet of such an incubated mixture was then dropped onto one cleaned quartz substrate and then another quartz plate was directly put on the droplet to have an extra thin and uniform object layer.

Characterization

Crystal morphologies and structures were characterized with a field-emission scanning electron microscope (FE-SEM, JEOL 6500), a field-emission transmission electron microscope (FE-TEM, JEOL-2100), a transmission electron microscope (TEM, Philips CM20) and X-ray diffraction (XRD, Siemens D500, Cu-Kα radiation). The F127 structure (high concentration) of the lyotropic liquid crystalline phase was determined from the relative positions of the small-angle X-ray scattering (SAXS, Bruker NAVO-1/12-21) peaks. The SERS spectra were recorded using a Raman spectrometer (Jobin Yvon, Labram HR model) equipped with a nitrogen-cooled CCD detector and a He-Ne laser line (633 nm). Three scans were taken with 2 s accumulation time for each scan.

Results and discussion

1.1 Houseleek-like Ag nanocrystals grown with only AsA (#1)

Fig. 1(a) shows the SEM image of novel houseleek-like Ag nanocrystals grown in the presence of a high AsA concentration where the molar ratio of AsA to $AgNO_3$ was 10 to 1 (see Table 1). As addressed above, the presence of only AsA in the $AgNO_3$ aqueous solution will lead to a fast non-equilibrium reduction and nucleation procedure that has been well established as a key point for the growth of branched Ag nanocrystals. As displayed in the studies of Wang *et al.*,[5] branched Ag structures can only be found when the AsA molar ratio is 2 to 20 times higher than that of $AgNO_3$. In addition, the fine morphology of the formed

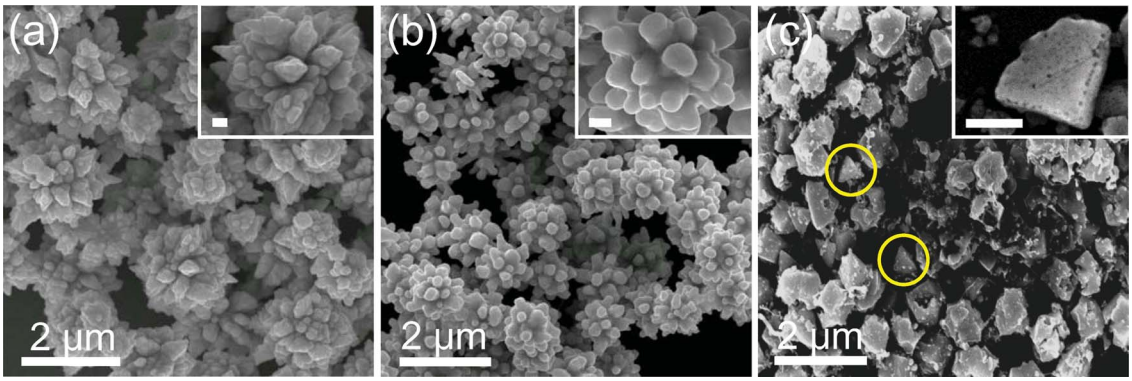

Fig. 1 SEM images of (a) houseleek-like Ag nanocrystals obtained with AsA only, (b) coral-like Ag nanocrystals obtained when F127 was added immediately after AsA addition, and (c) multi-faceted Ag nanocrystals obtained in the presence of F127 only. Inset: scale bar = 200 nm.

Table 1 Experimental parameters and resulting morphologies of Ag nanocrystals. (Final concentration in mM)

No.	AsA	F127	$AgNO_3$	Morphologies
#1	20	—	2	Houseleek-like spheres
#2	20	2[a]	2	Coral-like spheres
#3	—	2	2	Multi-faceted spheres
#4	20	2	2	Dendrites
#5	20	2	0.2	Dendrites
#6	20	10	2	Hexagonal prisms
#7	20	10	0.2	Triangular prisms

[a] Adding of AsA first followed by F127.

branches greatly depends on the molar ratio of AsA to $AgNO_3$ as well as the overall reagent concentrations. The present morphology (AsA:$AgNO_3$ = 10 : 1) further confirms suitable conditions for Ag short-branch growth. However, a closer look at the inset of Fig. 1(a) reveals that such houseleek-like morphologies consisting of an extremely high degree of branching and sharp tips have not been reported yet. Wang *et al.*[5] observed the very initial growth stages (from 3 s to 5 min) of Ag branches induced by AsA and concluded that branch formation basically follows two steps: the initial bulbous nucleation and the following reduction of Ag ions at the tips of the nuclei. Their description seems reasonable for the growth of branched crystals but cannot explain why Ag ions are selectively reduced on branch tips instead of other positions, or why the branch tips are morphologically different, such as sharp and round splitting tips, among others. Ben *et al.* experimentally and theoretically demonstrated that the tip morphology, *i.e.*, sharp tips or splitting tips, in diffusion-controlled crystal growth systems was the competitive result between the growth rates induced by the surface tension and kinetic effects respectively.[21] With the appearance of a lower or higher driving force, such as the undercooling degree for solidification, morphology tends to form surface-tension-dominated or kinetic-dominated needle tips, respectively. For the driving force between these two regions, the tips tend to have a splitting round shape.

In the present work, an especially high AsA concentration of 20 mM was introduced to provide a very strong driving force for fast nucleation of Ag ions. Due to the much higher nucleation rate than the growth rate, the formed Ag nuclei immediately aggregated to form spherical-like and dense-packed aggregates, but with numerous hemispheric tips (primary nuclei) at the very initial stage. After a large consumption of Ag ions at the fast nucleation stage, the residual Ag ions started the diffusion- controlled anisotropic growth step on previously formed round tips to form very sharp tips, as can be seen in Fig. 1(a). These sharp tips can be explained by the studies of Ben *et al.*,[21] which considered the effects of a higher growth driving force (kinetic effects), *i.e.*, the presence of the strong reductant AsA in the current case. Observing the morphology synthesized with an AsA and $AgNO_3$ concentration of 32 and 1.6 mM, respectively, by Wang *et al.*,[5] the sphere-like particles with short and sharp tips agree with our proposed two-step growth mechanism.

In addition, the porous dendritic branches and splitting tips were formed at a relatively low AsA and $AgNO_3$ concentration of 4.6 and 0.23 mM, respectively.[5] Under this condition, great aggregation should not occur and much smaller nuclei were thus obtained. After nucleation and aggregation, the diffusion-controlled growth process started and was dominated by the splitting tip growth due to the relative low driving force (lower AsA concentration), as predicted by the studies of Ben *et al.*[21]

1.2 Coral-like Ag nanocrystals grown with AsA first followed immediately by F127 (#2)

Fig. 1(b) shows the coral-like Ag nanocrystals synthesized by adding AsA first followed immediately by F127 to have a final concentration of 0.2 mM as listed in Table 1. The time difference between the additions of AsA and F127 was less than 5 s. Before adding F127, the formation mechanism of the crystals should be the same as that of the houseleek-like ones, *i.e.*, involving the fast nucleating and densely aggregating processes to form spherical-like crystals. F127 is a symmetrical tri-block copolymer with the central block of hydrophobic PPO sandwiched between blocks of more hydrophilic PEO. Since the critical micelle temperature (cmt) for 0.2 mM of F127 aqueous solution is around 21.5 °C,[22] the adding of F127 at a final concentration of 0.2 mM at room temperature should certainly produce spherical micelles, consisting of a relatively compact PPO core and a well solvated PEO shell in the solution and on the surface of previously formed Ag aggregates.

It has been well demonstrated that the PEO blocks in copolymers act as the catcher and reductant to form metallic nanoparticles.[23–26] However, these reducing processes generally require external energies, such as UV irradiation and heat, and have quite a long reaction time ranging from a few hours to a few days. It is thus reasonable to believe that the reduction of Ag ions is dominated by AsA instead of F127 due to not only its reduction ability but also the great difference in concentration between AsA and F127 (10 : 1). Although F127 cannot meaningfully contribute to the reduction of Ag ions, the SEM images in Fig. 1(a) and 1(b) suggest that F127 actually plays an important role in controlling the morphology of the reduced Ag crystals. In our experimental experience, the viscosity of the aqueous solution significantly increases even after adding a very small amount of F127 as also has been observed.[27] The formation of micelles will further increase the solution viscosity because of the extremely high solvation of the PEO shell.[28] As shown by the study of Ben *et al.*,[21] an increase in solution viscosity directly decreases the growth velocity resulting from the kinetic effect, thus producing splitting and round tips. Here, we can conclude that the splitting and round tips displayed in the inset of Fig. 1(b) presumably originates from the increase in viscosity caused by the F127 micelles and unimers.

1.3 Multi-faceted Ag nanocrystals grown in the presence of only F127 (#3)

For comparison purposes, Ag ions were reduced in the presence of only 0.2 mM F127 at room temperature. As described above, F127 micelles form and the PEO shell acts as the reductant to nucleate and then grow Ag crystals. As can be seen in Fig. 1(c), the formed Ag crystals exhibit multi-faceted morphology, indicating not only good crystallinity but also the equilibrium growth process produced by the weak reducing ability of F127. Similar multi-faceted metallic crystals formed by block copolymers can also be found elsewhere.[29,30] In addition, taking a closer look at Fig. 1(c), some triangular structures of flat surfaces can be clearly found (as marked in Fig. 1(c) and inset). Thus, the PEO blocks might also act as a capping reagent as reported earlier.[31] The scheme of the growth of above quasi-spherical nanocrystals (Fig. 1(a)–1(c)) is summarized in Fig. 2.

1.4 Dendritic Ag nanocrystals grown in the presence of both AsA and F127 micelles (#4 & #5)

The above results clearly indicate that block copolymers can perform single or multiple roles, such as acting as a reductant, a capping reagent, a stabilizer as well as a template, among others.[32–35] They can also be involved in crystal synthesis and morphology control mainly due to their temperature- and concentration-dependent chemical and physical features, as has been illustrated. The reduction ability of AsA for aqueous metallic ions is rather strong and thus the nucleation and growth processes are almost complete within an extremely short time period. To utilize the features of F127 well at the very initial growth stage, AsA and F127 was simultaneously introduced at different ratios to investigate their cooperative effects

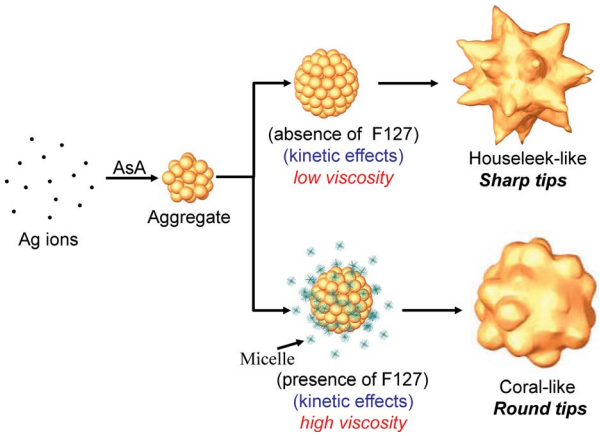

Fig. 2 Schematic of the proposed mechanism of houseleek-like and coral-like Ag nanocrystals.

on the growth of Ag crystals. Excluding the differences in $AgNO_3$, the condition of the present cases basically follows that of the coral-like Ag crystals as listed in Table 1 (#4 and #5). As can be seen in Fig. 3(a), the sharp XRD peaks recorded from the formed Ag crystals were indexed as the face-centered cubic Ag (JCPDS 4-783), clearly displaying high crystallinity and random stacks.

Fig. 3(b) and 3(c) show the SEM images of the prepared Ag crystals (#4). It is surprising that although the conditions are completely the same as those for the coral-like crystals (#2), the present morphologies are obviously different from the short-branched structure and exhibit very long dendritic structures just because of the simultaneous addition of F127. As can be seen in Fig. 3(b), the dendritic Ag crystals exhibit 3-D dendritic

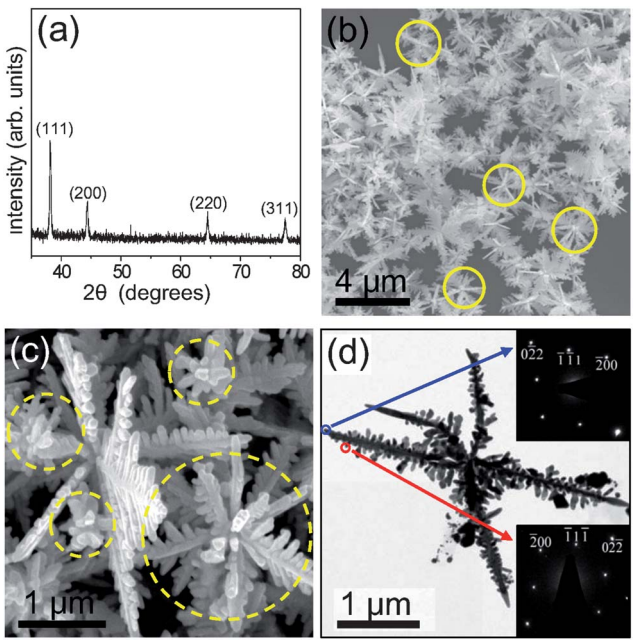

Fig. 3 (a) The XRD pattern, (b)–(c) SEM images and (d) TEM image of dendritic Ag nanocrystals (Inset: SAED patterns from the corresponding areas).

structures (3DDs) with a very high formation yield, branch density and structure uniformity in morphology and size. Fig. 3(c) clearly shows that the 3DDs are basically constructed with several long and straight backbones that uniformly radiate outward in 3-D and the secondary, even tertiary branches, are paralleled in 2-D. The estimated length and diameter of the central backbone of the 3DDs are 1.7 ± 0.3 μm and 0.1 μm, respectively. Further detailed examinations revealed that the secondary dendrites located at the base of the central backbone were much longer than those located at the tip (from approximately 300 nm (tip) to 600 nm (base) in length and with a similar width of ~100 nm), indicating the simultaneous growth of the central backbone and the secondary and tertiary dendrites. In addition, some relatively small dendrites that have no secondary or tertiary branches (as marked in Fig. 3(c)) are very similar to those of the coral-like structures (Fig. 1(b)), presumably giving us important hints regarding the growth mechanism. Fig. 3(d) shows the TEM image of an isolated Ag 3DDs and the selected area electron diffraction (SAED) from the tip of one central backbone and one secondary branch. The SAED patterns were obtained from an electronic beam along the [011] zone axis and proved the single crystal growth along <111> and <200> for the backbone and secondary branch, respectively.

To determine the influence of $AgNO_3$ concentration, which is a prerequisite for controlling the synthesis of silver nanocrystals with different morphologies as is widely reported,[6] we kept the concentrations of F127 and AsA the same but decreased $AgNO_3$ concentration from 2 to 0.2 mM (#5). Fig. 4 shows the SEM and TEM images of the typical morphology obtained in this experimental condition. As expected, the 3DDs were still formed. Interestingly, except the bare main backbones with a length of approximately 800 nm, the secondary and tertiary branches significantly disappeared, probably due to the consumption of $AgNO_3$ in the reaction system. Furthermore, the SAED patterns of one central backbone showed a single crystal growth along <111>.

By adding Ag ions, the ions are reduced mainly by AsA because of the much stronger reducing ability of AsA than that of F127 to form numerous Ag clusters. However, since F127 micelles (2 mM at room temperature) and some residual F127 monomers appear at the beginning of the growth process, we believe that they tend to cap the formed Ag clusters to greatly inhibit the growth rate as well as the aggregation of the Ag clusters.[23,36] It is thus reasonable to consider that the Ag aggregates should have only very few Ag clusters in contrast to the numerous clusters seen in Fig. 1(a) and 1(b). Each cluster at the surface of the very tiny aggregate formed possibly acts as the starting point of one isolated dendrite. By carefully checking the SEM and TEM images in Fig. 3 and 4, it is clear that dendritic growth starts from the very initial growth stages, which supports the proposal that the relatively small central core is due to the presence of both AsA and F127.

As described in Fig. 1, the presence of only AsA provides a very strong driving force and thus, elicits anisotropic growth with sharper tips. The subsequent adding of F127 effectively decreases the driving force (kinetic effects) and thus, leads to splitting round tips. From the careful observation of tip morphology in Fig. 3 and 4, most tips were round but some splitting round tips were also observed. Under the frame of Ben's model,[21] we believe that the anisotropic growth with round tips originates from the decrease in the kinetic effects generated by the existence of F127. The scheme of the formation of these 3DDs is shown in Fig. 5.

1.5 Triangular and hexagonal Ag prisms in the presence of both AsA and fcc-packed F127 micelles (#6 & #7)

In section 1.4, the formation of extremely long backbones and well-ordered secondary and tertiary branches required the presence of both AsA and a relatively low concentration of F127; however, we could not find any direct or convincing indirect evidence that F127 micelles act as a reductant or a growth director. In this section, we increased the F127 concentration from 2 to 10 mM to understand the role of face-centered-cubic (FCC) packed F127 micelles in growth. Fig. 6 shows the small angle X-ray scattering (SAXS) pattern recorded from pure F127 gel (10 mM) and the length ratio obtained from the second, third and fourth peak was $1 : \sqrt{2} : \sqrt{4}$, which was consistent with FCC packing (the first peak is overlapped with the direct beam). Fig. 7(a) and 7(d) display the TEM image of Ag triangular and hexagonal prisms obtained from the low and high concentrations of $AgNO_3$ (#7 and #6). A close look at Fig. 7(a) clearly displays a triangular-shaped planar body with a thinner edge. Fig. 7(b) shows the SAED pattern from the red circle area in Fig. 7(a). The SAED pattern can be indexed as the allowed {220} reflection (outer spots with a strong intensity) and formally forbidden 1/3

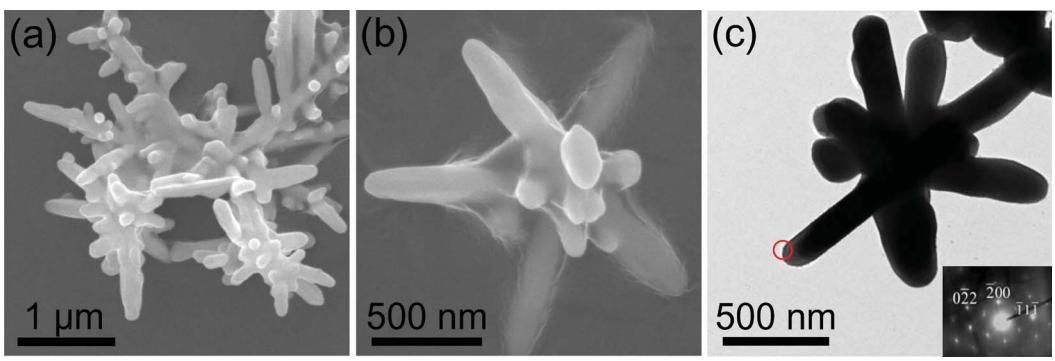

Fig. 4 (a)–(b) SEM images, and (c) TEM image of dendritic Ag nanocrystals grown at a low $AgNO_3$ concentration. (Inset: SAED pattern from the corresponding areas).

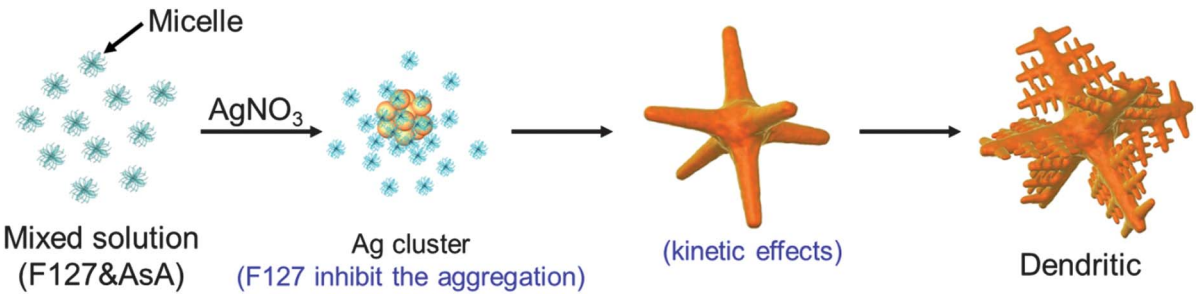

Fig. 5 Schematic of the proposed mechanism of dendritic Ag nanocrystals.

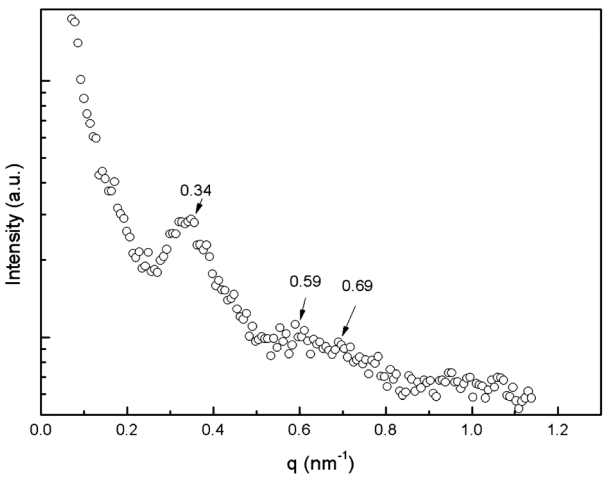

Fig. 6 The SAXS pattern of aqueous F127 (10 mM) at room temperature.

{422} reflection (inner sports with a weak intensity), indicating the [$\bar{1}$11] zone axis is normal to the top surface. The high-resolution TEM fringes of 0.25 nm (as seen in Fig. 7(c)) are also ascribed to the forbidden 1/3{422} reflection. Germain *et al.* demonstrated five possible structural models for the appearance of the forbidden 1/3{422} reflections in Ag hexagonal nanodisks.[37] Although the exact model could not be determined for the present triangular structure due to the lack of tilt-angle-resolved high-resolution TEM data, the appearance of the 1/3{422} reflection was reasonable for the observed disk-like structure (Fig. 7(a)) of a triangular-shaped planar body with a thinner edge. Fig. 7(e) shows the corresponding SAED pattern of one corner of the hexagonal prism. The square and circle marked spots can be indexed as {220} and the formally forbidden, 1/3{422} respectively, indicating that [$\bar{1}$11] is normal to the flat surface of the hexagonal prism.[37] The *d* spacing of 0.25 nm (as seen in Fig. 7(f)) is consistent with the spacing of the forbidden 1/3{422} described in Fig. 7(c).

Wang *et al.* reported that silver nanoparticles are almost reduced over the outer region to form hollow cylinders, *i.e.* a PPO core and an Ag particle-assembled shell, in the hexagonal packing of PEO-PPO-PEO micelles (75 wt% F127) in aqueous solution without any reductants.[9] These shell-distributed Ag nanoparticles seem to be related to the relatively rigid hydrophobic cores compared to the hydrophilic shell. In the present

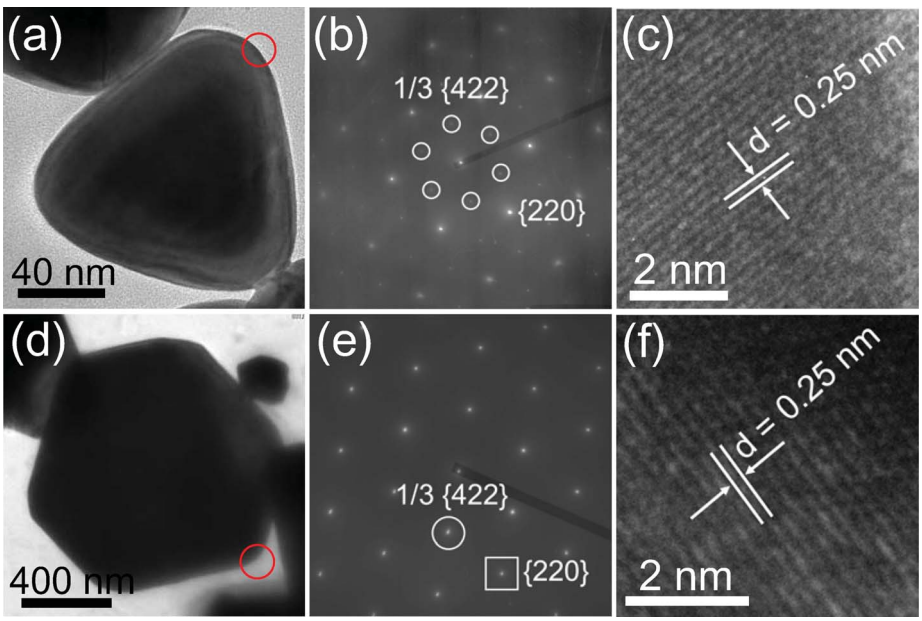

Fig. 7 TEM image of (a) triangular and (d) hexagonal Ag prisms. (b) & (c) and (e) & (f) are SAED patterns and high-resolution TEM images of region in (a) & (d), respectively.

FCC packed F127 micelles, since AsA was introduced, it is very reasonable to consider that Ag ions were rapidly reduced in two possible regions within these packed micelles, *i.e.*, the hydrophilic shell and the tetrahedral and octahedral voids constructed by FCC packing. These regions not only act as nano-reactors to provide reduction space or nucleation points for Ag ions, but also induce anisotropic growth due to the contamination of polymers on specific crystal planes. It is important to emphasize that with the assistance of the reductant AsA, the reduced Ag crystals exhibit distinct morphologies, such as triangular and hexagonal prisms, compared to all the Ag particles (approximately 500 nm) reduced by F127 without any reductants.[9] Although triangular and hexagonal Au nanoplates can also be formed under a specific concentration ratio of Au precursors to PEO-PPO-PEO block- copolymers in the absence of reductants,[30] the special round-edged triangular and hexagonal Ag prisms (see Fig. 7(a) and7(d)) reduced by AsA are probably regulated by different mechanisms.

As described above, the various highly branched structures showing porous constructions, larger surface areas, and sharper tips or edges could serve as great media for enhancing SERS detection.[38–40] The morphological disruption of noble or transition metals thus becomes an important research topic in SERS sensors.[41,42] Fig. 8 shows significant SERS enhancement of two types of the prepared Ag nanocrystals, respectively exhibiting short and long branches, for sensing MG molecules. The normal Raman spectra from the water-suspended 3DDs Ag nanocrystals and the pure MG aqueous solution are shown in Fig. 8(a) and (b), respectively. The main characteristic peaks of MG as marked by dashed lines are extremely weak even under such a high MG concentration (0.01 M). It is thus obviously difficult to provide reliable and reproducible data without further enhancement. With introducing the houseleek-like and 3DDs Ag nanocrystals into the MG aqueous solutions, significant SERS enhancements can be clearly found as observed in Fig. 8(c) and 8(d), respectively. An about 2 orders stronger Raman signal enabled by the 3DDs indicates the correct and effective strategies in developing 3-D and highly branched crystals for SERS related biological sensing and labeling applications.

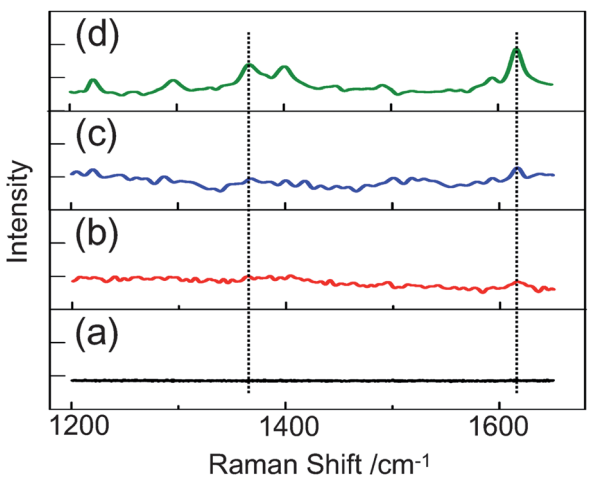

Fig. 8 Raman spectra from (a) the water-suspended 3DDs Ag nanocrystals without MG and (b) the MG aqueous solution. SERS spectra from (c) houseleek-like and (d) 3DDs Ag nanocrystals in MG aqueous solution. The intensity scale is 100, 100, 1000, and 10 000 counts per division in (a), (b), (c), and (d), respectively.

Conclusions

We successfully demonstrated that silver nanocrystals with various regulated morphologies were obtained by adjusting the relative concentration of F127, AsA and Ag precursors, as well as by changing the addition sequence at room temperature. At a lower concentration of F127 (2 mM) and in the presence of AsA, we synthesized three-dimensional dendritic Ag crystals with very long and ordered branches in a non-equilibrium system and demonstrated that higher $AgNO_3$ concentrations elicited the growth of higher-order dendrites compared to one-order branches produced by lower concentrations. When the F127 concentration was highly increased up to FCC packing, special hexagonal and triangular Ag prisms were obtained. In addition to these Ag crystals formed in the pre-mixed F127 and AsA, two types of short-branched Ag quasi-spheres, houseleek-like and coral-like structures, were also produced due to the domination of the AsA that was added before the F127. The present facile method demonstrated that the tri-block PEO-PPO-PEO copolymer indeed plays a very important and effective role in directing and developing various unusual morphologies with short and long 3D branches. The possible formation mechanisms of these structures were also proposed according to the structural investigations. The comparable excellent morphology-dependent SERS enhancement for both short and long types of branched structures in detecting MG molecules in aqueous solution indicates the merit of the tri-block copolymer mediated synthesis of Ag nanocrystals for liquid-based SERS sensors.

Acknowledgements

Financial support from the National Science Council of the Republic of China under grant NSC-99-2221-E-009-010 is gratefully acknowledged.

Notes and references

1 V. M. Cepak and C. R. Martin, *J. Phys. B*, 1998, **102**, 9985.
2 B. Wiley, Y. Sun, B. Mayers and Y. Xia, *Chem.–Eur. J.*, 2005, **11**, 454.
3 Y. Sun, B. Mayers and Y. Xia, *Nano Lett.*, 2003, **3**, 675.
4 X. W. Lou, C. Yuan and L. A. Archer, *Chem. Mater.*, 2006, **18**, 3921.
5 Y. Wang, P. H. C. Camargo, S. E. Skrabalak, H. Gu and Y. Xia, *Langmuir*, 2008, **24**, 12042.
6 T. Fukuyo and H. Imai, *J. Cryst. Growth*, 2002, **241**, 193.
7 X. Zheng, L. Zhu, A. Yan, X. Wang and Y. Xie, *J. Colloid Interface Sci.*, 2003, **268**, 357.
8 X. Wang, H. Kawanami, N. M. Islam, M. Chattergee, T. Yokoyama and Y. Ikushima, *Chem. Commun.*, 2008, 4442.
9 L. Wang, X. Chen, J. Zhao, Z. Sui, W. Zhuang, L. Xu and C. Yang, *Colloids Surf., A*, 2005, **257–258**, 231.
10 K. Niesz, M. Grass and G. A. Somorjai, *Nano Lett.*, 2005, **5**, 2238.
11 M. A. R. Meier, M. Filali, J. F. Gohy and U. S. Schubert, *J. Mater. Chem.*, 2006, **16**, 3001.
12 S. Forster and M. Antonietti, *Adv. Mater.*, 1998, **10**, 195.
13 S. A. Jenecke and X. L. Chen, *Science*, 1999, **283**, 372.
14 J. Y. Wang, W. Chen, C. Roy, J. D. Sievert and T. P. Russell, *Macromolecules*, 2008, **41**, 963.
15 M. Zhang, M. Drechsler and A. H. E. Muller, *Chem. Mater.*, 2004, **16**, 537.
16 P. Holmqvist, P. Alexandridis and B. Lindman, *J. Phys. Chem. B*, 1998, **102**, 1149.

17 L. M. L. Marzan and I. L. Tourino, *Langmuir*, 1996, **12**, 3585.
18 D. Zhang, L. Qi, J. Ma and H. Cheng, *Chem. Mater.*, 2001, **13**, 2753.
19 X. Gao, G. Gu, Z. Hu, Y. Guo, X. Fu and J. Song, *Colloids Surf., A*, 2005, **254**, 57.
20 L. Wang and Y. Yamauchi, *J. Am. Chem. Soc.*, 2009, **131**, 9152.
21 E. B. Jacob, P. Garik, T. Mueller and D. Grier, *Phys. Rev. A: At., Mol., Opt. Phys.*, 1988, **38**, 1370.
22 P. Alexandridis, J. F. Holzwarth and T. A. Hatton, *Macromolecules*, 1994, **27**, 2414.
23 T. Sakai and P. Alexandridis, *Langmuir*, 2004, **20**, 8426.
24 L. Bronstein, E. Kramer, B. Berton, C. Burger, S. Forster and M. Antonietti, *Chem. Mater.*, 1999, **11**, 1402.
25 T. Sakai and P. Alexandridis, *J. Phys. Chem. B*, 2005, **109**, 7766.
26 S. Chen, C. Guo, G. H. Hu, J. Wang, J. H. Ma, X. F. Liang, L. Zheng and H. Z. Liu, *Langmuir*, 2006, **22**, 9704.
27 T. Vetter, M. Mazzotti and J. Brozio, *Cryst. Growth Des.*, 2011, **11**, 3813.
28 G. Wu, Z. Zhou and B. Chu, *Macromolecules*, 1993, **26**, 2117.
29 J. U. Kim, S. H. Cha, K. Shin, J. Y. Jho and J. C. Lee, *Adv. Mater.*, 2004, **16**, 459.
30 T. Sakai and P. Alexandridis, *Nanotechnology*, 2005, **16**, S344.
31 A. Mayer and M. Antonietti, *Colloid Polym. Sci.*, 1998, **276**, 769.
32 L. Wang, H. Wang, Y. Nemoto and Y. Yamauchi, *Chem. Mater.*, 2010, **22**, 2835.
33 S. Guo, J. Li, S. Dong and E. Wang, *J. Phys. Chem. C*, 2010, **114**, 15337.
34 L. Wang and Y. Yamauchi, *Chem. Mater.*, 2011, **23**, 2457.
35 P. Alexandridis and M. Tsianou, *Eur. Polym. J.*, 2011, **47**, 569.
36 T. Sakai and P. Alexandridis, *Langmuir*, 2005, **21**, 8019.
37 V. Germain, J. Li, D. Ingert, Z. L. Wang and M. P. Pileni, *J. Phys. Chem. B*, 2003, **107**, 8717.
38 L. Lu, A. Kobayashi, K. Tawa and Y. Ozaki, *Chem. Mater.*, 2006, **18**, 4894.
39 G. C. Schatz, *Acc. Chem. Res.*, 1984, **17**, 370.
40 X. Wen, Y. T. Xie, M. W. C. Mak, K. Y. Cheung, X. Y. Li, R. Renneberg and S. Yang, *Langmuir*, 2006, **22**, 4836.
41 H. Liang, Z. Li, W. Wang, Y. Wu and H. Xu, *Adv. Mater.*, 2009, **21**, 4614.
42 S. Boca, D. Rugina, A. Pintea, L. B. Tudoran and S. Astillean, *Nanotechnology*, 2011, **22**, 055702.

